Instability nature of the swirl appearance in liquid cones

Vladimir Shtern and Antonio Barrero
Department of Energy Engineering and Fluid Mechanics, University of Seville, E-41012 Seville, Spain
(Received 24 June 1994)

We study the nature of the swirl dynamo (the appearance of rotation in primarily nonswirling flows) that has been found in liquid conical menisci of electrosprays. A previous theory models the phenomenon in terms of the conical similarity solutions of the Navier-Stokes equations and reveals the appearance of swirling secondary regimes through the supercritical pitchfork bifurcation at threshold Reynolds number Re_*. The similarity solution can approximate a real flow only outside the vicinities of the apex and the capillary rim, i.e., in some region $r_i < r < r_o$, where r is the distance from the cone apex. The problem is how deviations from this solution at $r = r_i$ and $r = r_o$ influence the flow inside that region. It is shown here that for $\mathrm{Re} < \mathrm{Re}_*$, the deviations from the primary flow decrease far from both the boundaries, but for $\mathrm{Re} > \mathrm{Re}_*$, a swirl disturbance given at $r = r_o$ grows as r decreases until saturation at the secondary similarity solution. The swirling regime is found to be stable with respect to these spatially developing, steady, rotationally symmetric disturbances in a wide range of Re. Thus, the swirl comes from a near-capillary region, but its cumulation inside the cone occurs only for $\mathrm{Re} > \mathrm{Re}_*$.

PACS number(s): 47.15.−x, 47.20.Ky, 66.60.+a

I. INTRODUCTION

The generation nature of strong vortices—from the bathtub vortex to astrophysical swirling jets—is not absolutely clear yet. Recently, the appearance of intense swirls has been observed in the so called Zeleny-Taylor cones related to electrosprays. Zeleny [1] found that a meniscus of a conducting liquid at the exit of a capillary tube takes a conical shape when the tube is charged to a sufficiently high potential. Taylor [2] explained that this shape is due to a balance between the electrical pressure and surface tension forces when the liquid is at rest. In a small vicinity of the cone apex, destruction of the liquid surface takes place and a thin jet or spray erupts; the jet diameter may be 10^3 and more times less than the inner diameter of the capillary tube [3]. This phenomenon has drawn the attention of many researchers because of a wide and rapidly growing area of electrospray applications. As a result, striking new features have been revealed. In contrast to earlier conjectures that the flow inside the cone is always unidirectional—from the capillary to the cone apex, experiments have revealed a circulatory meridional motion [4]. This circulation is driven by surface shear stresses induced by the electric field since the liquid surface is not exactly equipotential. Moreover, there are observations of swirl appearance inside the menisci, and the rotation can be rather strong [5] (see also the photographs in this paper).

To model this phenomenon, a theoretical approach has been developed [6] using the conical similarity solutions of the Navier-Stokes equations. The supercritical pitchfork bifurcation of a secondary self-swirling regime has been found at a moderate intensity of the primary pure meridional motion. The similarity relation for the driving stresses, $\tau \sim 1/r^2$, is an approximation of a real distribution. Justification and limitations of this approximation are discussed in detail in [5]. The similarity model drastically eases the analysis but retains the effect of unforced generation of swirl observed in the experiment. What is the origin of the angular momentum corresponding to this bifurcation? Some alternative conjectures have been made in [5,6], and the aim of our paper is to illuminate this problem. For this we study the spatial stability of the similarity solutions.

In the similarity class, all velocity components are inversely proportional to distance r from the coordinate origin, positioned here at the cone apex. Due to the singularity, the similarity solution cannot be applied in some vicinity, $r < r_i$, of the apex. Also the no-slip condition at the wall and the cylindrical geometry of the capillary tube are incompatible with the conical similarity. Therefore, one may use the similarity solution only in the range, $r_i < r < r_o$ where r_o is smaller than the distance of the capillary rim from the apex. One more condition for this similarity—$r_o/r_i \gg 1$—is often fulfilled in Zeleny-Taylor cones, as we mentioned above.

Since some deviations from the similarity solution are unavoidable at $r = r_i$ and $r = r_o$, the question arises as to how these deviations influence the flow inside the range. They can decay far from the boundaries or amplify and totally destroy the similarity. Therefore, a study of the sensitivity to these deviations is needed to determine whether or not similarity solutions are able to approximate real flows. If the answer is positive, the analysis provides estimations of the Reynolds number diapason where the solutions are valid and of what occurs at the diapason ends. Here we restrict ourselves to rotationally symmetric disturbances because this appears to be sufficient to understand the nature of the swirl bifurcation.

II. PROBLEM FORMULATION

We consider flows of a viscous incompressible fluid admitting the representation

$$v_r=\nu r^{-1}u(x,\xi)\ ,\quad v_\theta=\nu(r\sin\theta)^{-1}y(x,\xi)\ ,$$
$$v_\phi=\nu(r\sin\theta)^{-1}\Gamma(x,\xi)\ ,\quad p=p_\infty+\rho\nu^2r^{-2}q(x,\xi)\ ,$$
$$\xi=\ln(r/r_0)\ ,\quad x=\cos\theta\ , \tag{1}$$

where v_r, v_θ, and v_ϕ are the velocity components in the spherical coordinates (r,θ,ϕ); r is the distance from the origin; θ and ϕ are the polar and azimuthal angles (Fig. 1); p, ρ, and ν are pressure, density and kinematic viscosity; r_0 is a length scale to make the argument of the logarithm dimensionless.

Substitution of (1) in the Navier-Stokes equations reduces them to the system

$$(1-x^2)u_{xx}=(2x-y)u_x-u_{\xi\xi}-u_\xi+uu_\xi-u^2$$
$$-2q+q_\xi-(y^2+\Gamma^2)/(1-x^2)\ ,$$
$$(1-x^2)\Gamma_{xx}=u\Gamma_\xi-y\Gamma_x+\Gamma_\xi-\Gamma_{\xi\xi}\ ,$$
$$(1-x^2)q_x=(1-x^2)(u_x-u_{x\xi})+uy_\xi-yu_\xi-yu$$
$$+y_\xi-y_{\xi\xi}-x(y^2+\Gamma^2)/(1-x^2)\ ,$$
$$y_x=u+u_\xi\ , \tag{2}$$

for dimensionless functions u, y, Γ, and q, where indices denote differentiation with respect to the corresponding variables.

The conical boundary of the liquid meniscus, $x=x_c$, is considered impermeable and acted on by the given surface stresses,

$$\tau_{\theta r}=\rho\nu^2(r^2\sin\theta)^{-1}[y_\xi-2y-(1-x^2)u_x]$$

and

$$\tau_{\theta\phi}=-\rho\nu^2(r\sin\theta)^{-2}[(1-x^2)\Gamma_x+2x\Gamma]=0\ ,$$

that yield the boundary conditions

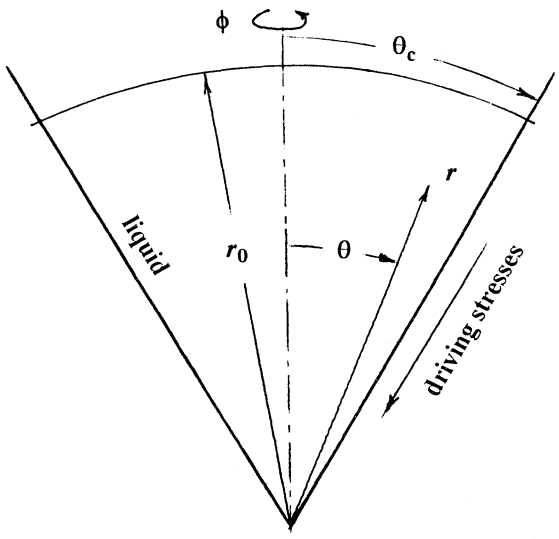

FIG. 1. Schematic of the problem. The coordinates and shear stresses are shown.

$$y=0\ ,\ (1-x^2)\Gamma_x+2x\Gamma=0\ ,\ (1-x_c^2)^{1/2}u_x=\mathrm{Re}_\tau$$
$$\text{at } x=x_c\ . \tag{3}$$

Dimensionless parameter $\mathrm{Re}_\tau=-r^2\tau_{\theta r}/(\rho\nu^2)$ characterizes the intensity of the surface forcing and is a kind of Reynolds number. The minus sign is used to make Re_τ positive when $\tau_{\theta r}$ is directed toward the origin (this direction is relevant in the context of this paper). The conditions at the symmetry axis,

$$y=0\ ,\ \Gamma=0\ ,\ 2u_x-u_{\xi\xi}-u_\xi+uu_\xi-u^2-2q+q_\xi=0$$
$$\text{at } x=1\ , \tag{4}$$

follow from (1), (2), and the requirement of velocity boundness. The above formulation is a generalization of that made in [6] for u, y, Γ, and q depending on two variables, x and ξ.

III. LINEAR STABILITY PROBLEM

Problem (2)–(4) has solutions independent of ξ, i.e., self-similar, that have been reported in [5,6] and are referred to here as basic. To study the spatial stability of the basic solutions with respect to small disturbances, we look for solutions of the form

$$u=u_b(x)+u_d(x)\exp(\alpha\xi)\ ,$$
$$y=y_b(x)+y_d(x)\exp(\alpha\xi)\ ,$$
$$\Gamma=\Gamma_b(x)+\Gamma_d(x)\exp(\alpha\xi)\ ,$$
$$q=q_b(x)+q_d(x)\exp(\alpha\xi)\ , \tag{5}$$

where subscripts b and d denote the basic and disturbance parts. The normal (exponential) form of the infinitesimal disturbances is adequate because the coefficients in (2)–(4) do not depend on ξ. Substituting (5) into (2) and neglecting nonlinear terms with respect to the disturbances, we get

$$(1-x^2)u_d''=(2x-y_b)u_d'+[(\alpha-2)u_b-(\alpha+\alpha^2)]u_d$$
$$-u_b'y_d+(\alpha-2)q_d-w\ ,$$
$$(1-x^2)\Gamma_d''=(\alpha u_b+\alpha-\alpha^2)\Gamma_d-y_b\Gamma_d'-\Gamma_b'y_d\ ,$$
$$(1-x^2)q_d'=(1-x^2)(1-\alpha)u_d'$$
$$+(1-\alpha)(\alpha-u_b)y_d-(1+\alpha)y_bu_d-xw\ ,$$
$$y_d'=(1+\alpha)u_d\ ,\quad w=2(y_by_d+\Gamma_b\Gamma_d)/(1-x^2)\ , \tag{6}$$

where the prime means differentiation with respect to x. The boundary conditions for the disturbances follow from (3)–(5) and are

$$y_d=0\ ,\ (1-x^2)\Gamma_d'+2x\Gamma_d=0\ ,\ u_d'=0\ \text{at}\ x=x_c\ ,$$
$$y_d=0\ ,\ \Gamma_d=0\ ,\ 2u_d'-[\alpha+\alpha^2-(\alpha-2)u_b]u_d$$
$$+(\alpha-2)q_d=0\ \text{at}\ x=1\ . \tag{7}$$

The perturbed shear stresses are zero at the liquid surface because Re_τ is not subject to disturbances. Problem (6),(7) has the trivial (zero) solution and we need to find

eigenvalues of α for nontrivial solutions to exist. We will see that there are eigensolutions corresponding to both the positive and negative α_r; subscript r denotes here the real part of a complex α. To ascertain the physical meaning of the eigenmodes, we consider first the stability of fluid at rest.

IV. STABILITY OF THE EQUILIBRIUM

For motionless fluid we expect any disturbances to decay. First, we consider disturbances given at $r=r_0$ inside the cone (see Fig. 1). We will study the disturbance propagation in regions $r>r_0$ and $r<r_0$ to classify what modes are relevant for these outer and inner problems.

When $\Gamma_b=u_b=y_b\equiv 0$, the equations for the swirl disturbance,

$$(1-x^2)\Gamma_d''=(\alpha-\alpha^2)\Gamma_d \ , \tag{8}$$

and the meridional motion disturbance,

$$\begin{aligned}&(1-x^2)u_d''=2xu_d'-(\alpha+\alpha^2)u_d+(\alpha-2)q_d \ ,\\ &(1-x^2)q_d'=(1-x^2)(1-\alpha)u_d'+(1-\alpha)\alpha y_d \ ,\\ &y_d'=(1+\alpha)u_d \ ,\end{aligned} \tag{9}$$

are decoupled. Since the boundary conditions (7) are also decoupled, one can treat these disturbances separately.

Equation (8) can be rewritten in the form

$$[(1-x^2)\Gamma_d'+2x\Gamma_d]'+(\alpha+1)(\alpha-2)\Gamma_d=0 \ . \tag{10}$$

Integration of (10) from $x=x_c$ to $x=1$, together with (7), yields

$$(\alpha+1)(\alpha-2)\int_{x_c}^{1}\Gamma_d dx=0 \ . \tag{11}$$

The eigensolutions $\Gamma(x)$ can be expressed in terms of the Legendre function (the Legendre polynomials for $\theta_c=\pi/2$ and $\theta_c=\pi$, when all eigenvalues of α are integer numbers). The spectrum of α is symmetric with respect to $\alpha=\frac{1}{2}$ and real. As θ_c decreases, $|\alpha|$ increases with the two following exceptions.

There are two special eigenvalues: (i) $\alpha=-1$ and (ii) $\alpha=2$ corresponding to $\Gamma_d=C(1-x^2)$, where C is a constant. These solutions are universal with respect to the cone angle and are also valid for an unbounded fluid, i.e., at $\theta_c=\pi$. Solution (i) provides the main term of a far field asymptotic expansion for the azimuthal velocity as $r\to\infty$. This term corresponds to the conservation law of the angular momentum for the flow in the region $r>r_0$. Solution (ii) provides the main term of a power-law expansion near $r=0$ for a flow inside the sphere $r=r_0$ and corresponds to the solid-body rotation at $r\ll r_0$.

Now we consider a flow inside region $r_i<r<r_o$, $r_o/r_i\gg 1$ (see Fig. 2) and, based on the above analysis, assume that (i) relates to the disturbance given at $r=r_i$ and decaying most weakly as r increases, while (ii) relates to the disturbance given at $r=r_o$ and decaying most weakly as r decreases. For other eigenmodes, the net circulation (i.e., the integral angular momentum) is zero as follows from (11).

Solutions of (9) can again be expressed in terms of the Legendre function (the Legendre polynomials for $\theta_c=\pi/2$ and $\theta_c=\pi$), and the corresponding spectrum of α is also symmetric with respect to $\alpha=\frac{1}{2}$ and real. The disturbances of the meridional motion are classified in the same way as the swirl disturbances; they are found to be less important in the context of this paper.

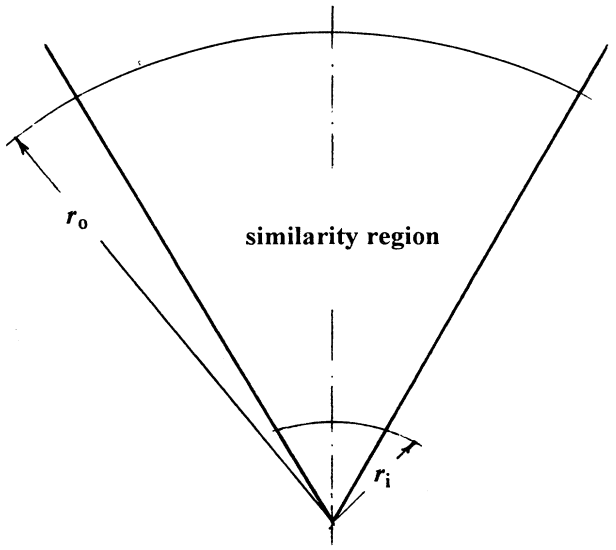

FIG. 2. Schematic of the similarity region.

Thus, a general solution for a velocity field in $r_i<r<r_o$ induced by disturbances given at the boundaries can be represented as $\Sigma_i+\Sigma_o$ where Σ_i is a superposition of the modes with $\alpha<0$ and provides a contribution of disturbances given at the inner boundary $r=r_i$, while Σ_o is a superposition of the modes with $\alpha>0$ and provides a contribution of disturbances given at the outer boundary $r=r_o$.

V. INSTABILITY OF THE PRIMARY REGIME

Now we will study the dependence on Re_τ of a few main eigenvalues for the primary nonswirling flow. The first change of α_r sign at $\mathrm{Re}_\tau=\mathrm{Re}_{\tau *}$, as Re_τ increases, is interpreted here as instability. When $d\alpha_r/d\,\mathrm{Re}_\tau>0$ at $\mathrm{Re}_\tau=\mathrm{Re}_{\tau *}$, the instability relates to the disturbances coming from $r=r_i$; when $d\alpha_r/d\,\mathrm{Re}_\tau<0$ at $\mathrm{Re}_\tau=\mathrm{Re}_{\tau *}$, the growing disturbance comes from the outer boundary. Since $\Gamma_b\equiv 0$, again the equations for the swirl disturbance,

$$(1-x^2)\Gamma_d''=(\alpha u_b+\alpha-\alpha^2)\Gamma_d-y_b\Gamma_d' \ , \tag{12}$$

and for the meridional motion disturbance,

$$\begin{aligned}(1-x^2)u_d''&=(2x-y_b)u_d'+[(\alpha-2)u_b-(\alpha+\alpha^2)]u_d\\ &\quad -u_b'y_d+(\alpha-2)q_d-w \ ,\\ (1-x^2)q_d'&=(1-x^2)(1-\alpha)u_d'\\ &\quad +(1-\alpha)(\alpha-u_b)y_d-(1+\alpha)y_bu_d-xw \ ,\\ y_d'&=(1+\alpha)u_d \ , \quad w=2y_by_d/(1-x^2) \ ,\end{aligned} \tag{13}$$

can be treated separately.

At $\alpha=-1$, integration of (12) yields

$$(1-x^2)\Gamma_d'+(2x+y_b)\Gamma_d=0 \ . \tag{14}$$

[The integration constant must be zero to satisfy the condition $\Gamma_d(1)=0$.] The boundary condition at the surface is fulfilled for any solution of (14) because $y_b(x_c)=0$. Applying the normalization, $\Gamma_d(x_c)=1$, we get the integral form of the solution

$$\Gamma_d=\exp\{-\int_{x_c}^{x}[(2x+y_b)/(1-x^2)]dx\} \ .$$

Therefore, $\alpha=-1$ is the eigenvalue for any Re_τ and x_c. This mode has the same physical meaning with respect to the angular momentum conservation as defined in case (i) of the preceding section. All other swirl disturbances given at $r=r_i$ decay faster as r increases, and asymptotically v_ϕ decays like r^{-2}. Thus no instability relates to the swirl disturbances coming from the inner boundary.

However, the situation is different for the swirl disturbances coming from the outer boundary. Except for the above analytical solutions, the problem has been solved numerically. Figure 3 shows the results for the two main positive (curves 1*o* and 2*o*) and negative (curves 1*i* and 2*i*) eigenvalues. At the abscissa we use $\mathrm{Re}=-rv_{rc}/\nu$, where v_{rc} is the radial velocity at the surface. This Reynolds number can be found after the problem of the basic flow is solved. For the primary regime, there is the explicit relation $\mathrm{Re}=\frac{1}{2}\mathrm{Re}_\tau[(1-x_c)/(1+x_c)]^{1/2}$.

Our main result is that curve 1*o* passes line $\alpha=0$ at $\mathrm{Re}=\mathrm{Re}_*=6.3$, which exactly corresponds to the bifurcation value obtained in [5]. This means that the bifurcation of the self-swirling regime occurs due to the instability of the primary flow under a disturbance coming from the outer boundary. For supercritical Re, curve 1*o* approaches, but does not touch, line 1*i* (i.e., $\alpha\equiv-1$); α decreases along curve 1*o* up to its minimum value, which is very close to, but larger than, -1 and then increases together with Re. When Re approaches $\mathrm{Re}^*=31.6$, where the collapse of the primary solution occurs [5–7], α tends to $\alpha^*\cong-0.5$ along curve 1*o*. The fact that $\alpha^*\neq0$ means that the growing mode has no tendency to become localized near the axis.

Other swirling modes do not relate to any bifurcation up to $\mathrm{Re}=\mathrm{Re}^*$. The same is valid for the meridional motion disturbances (see Fig. 4). The most weakly decaying mode of the disturbances coming from the inner boundary relates to curve 1*i* in Fig. 4. Although α increases, approaching zero as $\mathrm{Re}\to\mathrm{Re}^*$, it does not change its sign inside the interval $(0,\mathrm{Re}^*)$. The corresponding eigenmode becomes localized near the axis, i.e., this is a disturbance of the near-axis jet. The tendency of this eigenvalue to become zero at $\mathrm{Re}=\mathrm{Re}^*$ is related to the viscous nature of this mode and to the fact that the local Reynolds number, based on the axial velocity, tends to infinity as $\mathrm{Re}\to\mathrm{Re}^*$.

The eigenvalues for other modes presented in Fig. 4 do not remain real in this range of Re. As Re increases, first curves 2*i* and 3*i* merge at $\mathrm{Re}=5.7$ and then a complex conjugated pair of eigenvalues appears at $\mathrm{Re}>5.7$. The real and imaginary parts of α are shown in Fig. 4 by dashed curves 2*ir* and 2*ii*, respectively. At $\mathrm{Re}=7.1$, curves 1*o* and 2*o* merge and one more complex conjugated pair appears; the real and imaginary parts of α are shown in Fig. 4 by curves 1*or* and 1*oi*, respectively. At $\mathrm{Re}=10.4$, the two complex conjugated eigenvalues for the inner modes corresponding to curves 2*ir* and 2*ii* merge and these eigenvalues become again real at $\mathrm{Re}>10.4$ (see curves 2*i* and 3*i* in Fig. 4). We see that

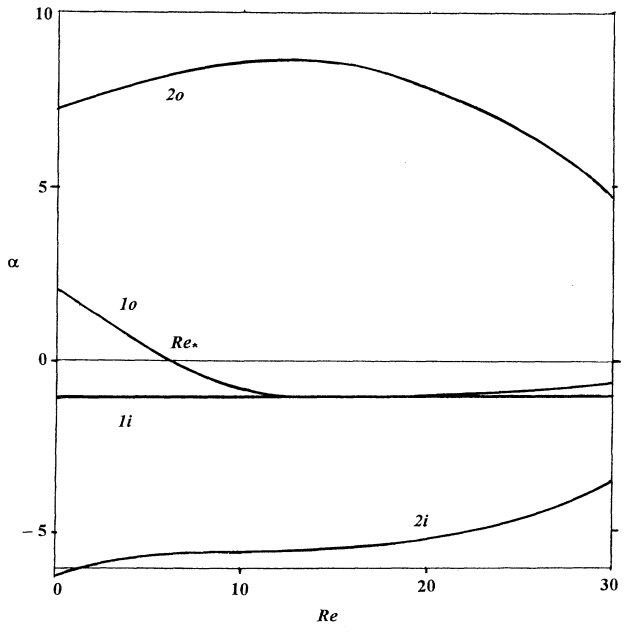

FIG. 3. Dependence of spatial growth rate α on the Reynolds number Re for swirl disturbances of the primary regime. $\theta_c=45°$.

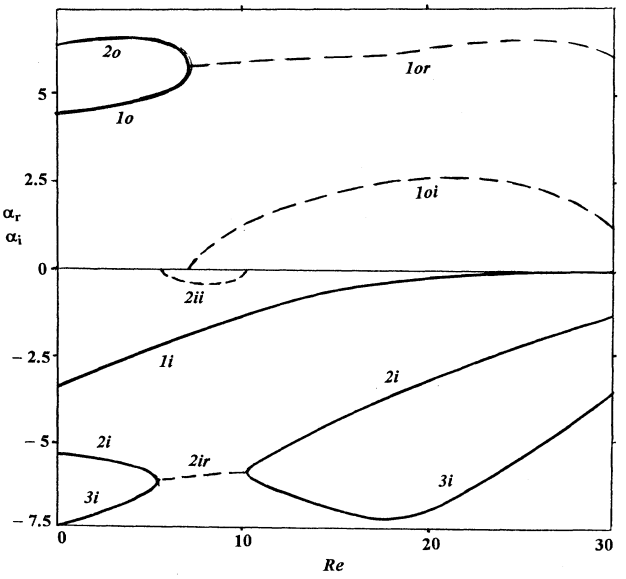

FIG. 4. The same as in Fig. 3, but for disturbances of the meridional motion.

there are rather sophisticated transformations of the spectrum as Re increases; however, this does not relate to any new bifurcation.

Thus there is a single mode of the swirl disturbance given at the outer boundary, $r=r_o$, that can be related to accumulation of the angular momentum near the apex when $\mathrm{Re}>\mathrm{Re}_*$. Now we shall study the nonlinear development of swirl as r decreases at Re slightly larger than Re_*.

VI. WEAKLY NONLINEAR EVOLUTION

In the supercritical vicinity of $\mathrm{Re}=\mathrm{Re}_*$, the weakly nonlinear stability theory [8,9] can be used to study the spatial evolution (as r decreases) of the growing mode up to its saturation at the secondary regime. Note that for the spatial instability of the planar conical flows, this theory is applied in [10,11], and there the growing disturbances develop from the origin as r increases, i.e., in the opposite direction to that in this case. We use the small parameter ε, $\mathrm{Re}_\tau=\mathrm{Re}_{\tau *}+\varepsilon^2$, and the expansion for the swirl,

$$\Gamma=\varepsilon A(\eta)\Gamma_d(x)+\varepsilon^2 A_2(\eta)\Gamma_{d2}(x)+\cdots,\quad \eta=-\varepsilon^2\xi\ , \tag{15}$$

where $\Gamma_d(x)$ is the eigenfunction for the neutral mode of the linear problem at $\mathrm{Re}=\mathrm{Re}_*$. The expansion for the meridional motion disturbance starts from the quadratic term with respect to ε, and the standard procedure [8–11] deduces [with the help of (2) and (15)] the Landau equation

$$dA/d\eta=\gamma A(1-A^2/A_s^2)\ ,\quad A(0)=A_o\ , \tag{16}$$

$$\gamma=-d\alpha/d\,\mathrm{Re}_\tau \text{ at } \mathrm{Re}=\mathrm{Re}_*\ .$$

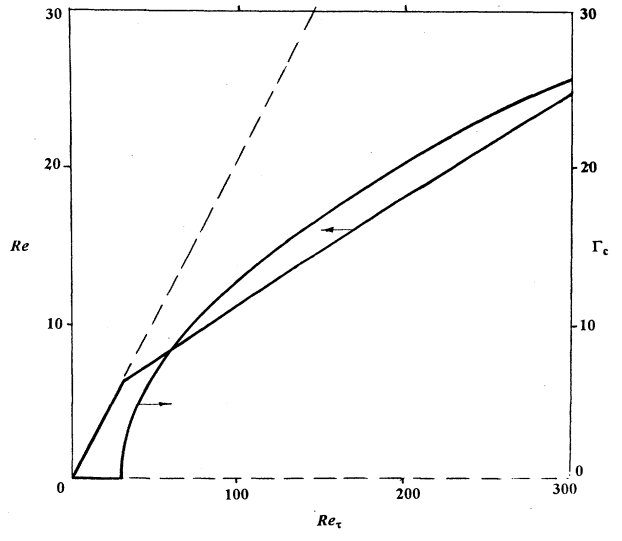

FIG. 5. Dependence of the radial velocity (Re) and circulation (Γ_c) on the surface shear stresses (Re_τ) for the similarity stable (solid lines) and unstable (dashed lines) solutions. $\theta_c=45°$.

Its solution, $A=A_o A_s \exp(\gamma\eta)[A_s^2-A_o^2+A_o^2\exp(2\gamma\eta)]^{-1/2}$, describes the whole nonlinear transition from the primary to the secondary similarity solution. The saturation amplitude A_s can be found from the solvability requirement for the circulation equation governing the terms of $O(\varepsilon^3)$. However, for this problem, it is easier to find A_s from the numerical calculations of the secondary similarity solution in the supercritical vicinity of $\mathrm{Re}=\mathrm{Re}_*$, which with the help of (15) and the normalization $\Gamma_d(x_c)=1$, gives $A_s=1.5$. Figure 5 shows the dependencies of Re and $\Gamma_c=\Gamma(x_c)$ on Re_τ for a rather wide supercritical range. The meridional motion is slower in the secondary regime than in the primary one for the same forcing (compare the solid and dashed lines in Fig. 5). This is due to the fact that some part of the kinetic energy of the meridional motion is transformed into rotational kinetic energy in the swirling regime.

VII. STABILITY OF THE SECONDARY REGIME

Considering the supercritical vicinity of $\mathrm{Re}=\mathrm{Re}_*$, we found that the instability of the primary similarity solution is related to the transition process that is established at the secondary similarity solution. In particular, this means that the secondary regime is stable. To check if this is also valid in some range of Re outside this vicinity, we need to solve the problem (6),(7) using the swirling regime as the basic solution. Since $\Gamma_b\neq 0$, the swirl and meridional disturbances are coupled now. To find the spectrum, we apply the following numerical procedure. Equations for the basic and disturbance solutions are integrated simultaneously from $x=1$ to $x=x_c$. To form the complete initial data at $x=1$, we choose some tentative values for the variables not specified at $x=1$. Then the tentative values are corrected by shooting to satisfy the boundary conditions at $x=x_c$. We use $\Gamma_b'(1)$ as a free parameter and start from $\Gamma_b'(1)=0$ at $\mathrm{Re}=\mathrm{Re}_*$, where the primary and secondary basic solutions coincide and, therefore, their disturbance spectra coincide, too. Then we gradually increase $\Gamma_b'(1)$ using the tentative values found for the previous parameter value as initial data for the shooting procedure. The (Newton) shooting procedure converged for a small enough step of the parameter.

Figure 6 shows the calculated results. Real eigenvalues of α correspond to the solid curves and α_r of the complex eigenvalues correspond to the dashed lines. For $\mathrm{Re}<\mathrm{Re}_*$, the spectrum of the primary solution that is inherited by the secondary solution at $\mathrm{Re}=\mathrm{Re}_*$ is shown, where all curves have jumps in their slope. Curve $1o$ corresponding to the main eigenvalue is reflected from the line $\alpha_r=0$ for the secondary solution. None of the curves passes the line $\alpha_r=0$ in Fig. 6, meaning that the self-swirling regime is stable with respect to this class of disturbances in this range of Re. The problem of the swirling regime stability with respect to more general, say, unsteady, three-dimensional, disturbances remains unresolved; however, we believe that there is a stability range of Re, because steady rotationally symmetric regimes are observed in experiments.

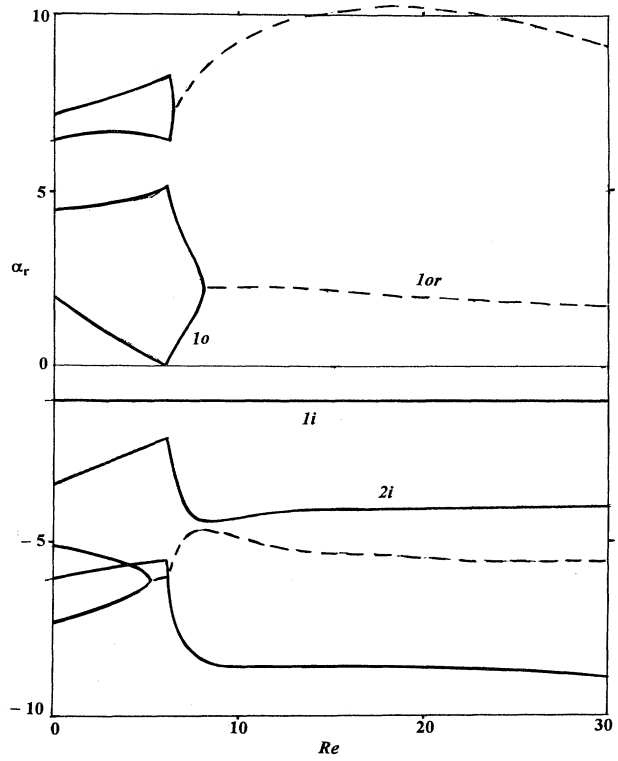

FIG. 6. The spatial stability spectrum for the secondary self-swirling solution. $\theta_c = 45°$.

VIII. OBSERVATION OF SWIRL IN TAYLOR CONES

To obtain the photographs given in Fig. 7 we have used the experimental setup typical for electrospray experiment. Usually the electroatomization technique consists of the slow injection of a liquid through a capillary—an electrified needle. For certain ranges of the applied voltage and liquid flow rate, one can find a special steady regime—the so called cone-jet mode [12]. In this regime, the liquid is emitted as an extremely thin charged jet from the vertex of an almost conical meniscus. Then the jet breaks up into a fine spray of droplets.

The experimental setup is sketched in Fig. 8. Pressurized air drives the liquid in reservoir A (a few cm^3 disposable syringe) through a narrow insulating Teflon tube B having a 0.32 mm inner diameter and a length ranging from a few to 20 meters. The tube ends up at a capillary needle C (of 1 mm inner diameter) charged at an electrical potential of a few kV relative to a flat ground electrode D. This electrode is positioned 2.5 cm from and perpendicular to the needle. Needle C and the liquid surface in reservoir A are kept at the same height to ease the flow rate measurements. Liquid flow rate Q is controlled by pressure in the reservoir, and voltage V is provided by a Bertan 250-10R High Voltage Power Supply E.

To have the relation, $Q = a\Delta p$, the pressure drop Δp across the feeding line must be much larger than the pressure jump at the meniscus interface (that is of order γ/d; γ is the surface tension and d is the needle diameter). Constant a is found from calibration measurements of Q and Δp. Q is measured by introducing an air bubble in the feeding line and timing its path, Δp is measured with a mercury manometer. Once a is calculated, the measured Δp directly yields Q.

The liquid in our experiments is ethanol or heptane doped with small amounts of an antistatic additive (Stadis 450, Du Pont) to enhance its electrical conductivity by several orders of magnitude without significantly changing other physical properties (such as surface tension, dielectric constant, and density). Very small droplets of milk and/or air bubbles are used as trace particles. A Nikkon Stereoscopic Microscope SM7-2T with a photographic tube has been used to make the photographs of the conical meniscus. The illumination of the meniscus is provided by two 50 W halogen lamps.

The liquid motion patterns in the meniscus are shown for heptane flow rate $Q = 5.5\times10^{-10}$ m^3/s, $V = 5.4$ kV [Fig. 7(a)] and nearly the same values for Fig. 7(b); $Q = 9\times10^{-10}$ m^3/s, $V = 5.2$ kV [Fig. 7(c)]; and ethanol flow rate $Q = 3\times10^{-10}$ m^3/s, $V = 5.5$ kV [Fig. 7(d)]. It is clear from the photographs that swirl increases from Fig. 7(a) to Fig. 7(d): swirl is practically absent in Fig. 7(a); the spiral trajectory of a bubble in Fig. 7(b) obviously shows the superposition of the meridional circulation and swirl; the bubble tracks nearly normal to the boundary of the cone projection show a rather strong swirl in Fig. 7(c); and, finally, swirl is so strong in Fig. 7(d) that the vicinity of the cone vertex seems twisted. Thus, the experiment supports the theoretical result that the critical Reynolds number exists separating nonswirling and swirling steady flow regimes.

IX. DISCUSSION

A. Elementary mechanism of the instability

We have found that bifurcation in the conical similarity solutions of the Navier-Stokes equations leading to appearance of rotation in the primarily nonswirling flows is related to instability with respect to swirl disturbances propagating from the outer boundary of the similarity region. The instability occurs when the Reynolds number Re characterizing the intensity of the meridional motion exceeds a critical value Re_*.

Figure 9 illustrates this situation. Let us suppose that at some distance $r = r_o$ from the apex of the canonical meniscus, say, near the capillary rim, a swirling disturbance is given and characterized by Γ_{co}, representing a circulation value at the liquid surface. When the meridional motion is very slow, i.e., $Re \ll Re_*$, the angular momentum propagates inside the cone mainly due to diffusion up to saturation at the solid-body-rotation type of circulation distribution, $\Gamma_c = \Gamma_{co}(r/r_0)^2$, shown by curve 1 in Fig. 9. In this case, the angular velocity is nearly uniform inside the cone and equals its value at $r = r_o$.

However, when $Re > Re_*$, convection plays an important role in the mechanism of swirl transport. If one neglects diffusion, then the angular momentum of a liquid

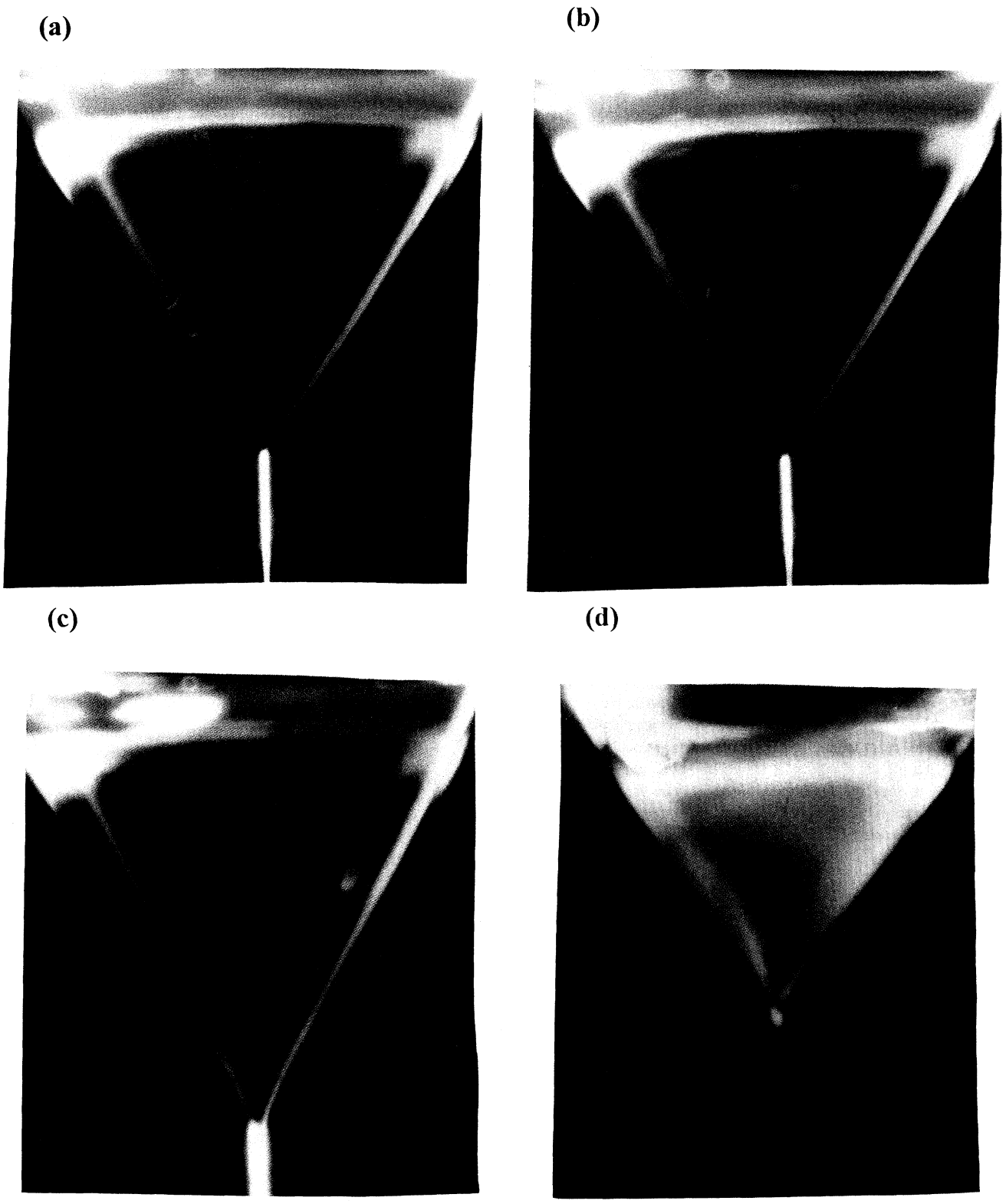

FIG. 7. Photographs of the nonswirling (a) and swirling (b)–(d) regimes in a Taylor cone.

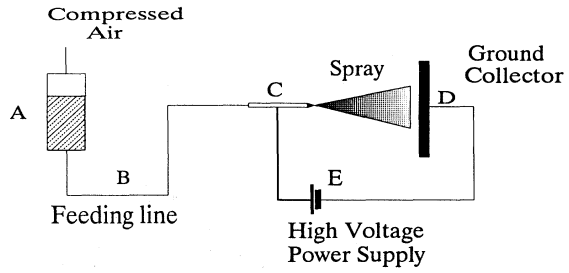

FIG. 8. Schematic of the experimental setup.

particle is conserved when the particle moves to the apex along the surface and, therefore, circulation would be constant along the trajectory. Due to the circulatory character of the meridional motion, the particle turns and moves from the apex along the axis. If again its circulation remains constant, then the azimuthal velocity of the particle becomes very large because the distance from the axis is small. Since the azimuthal velocity must be zero to the axis, a huge gradient of the angular momentum in the meridional direction is generated. This means that viscous diffusion of the angular momentum from the axis to the surface cannot be ignored even when $\mathrm{Re} \gg 1$. Thus, the mutual action of convection and diffusion induces the normal-to-streamline transfer of the angular momentum, increasing circulation of near-surface particles. For $\mathrm{Re} < \mathrm{Re}_*$, this increase is not sufficient to compensate for the loss of circulation due to the viscous diffusion along streamlines. At $\mathrm{Re} = \mathrm{Re}_*$, there is a balance of increase and loss, so the particle conserves is circulation when it moves from the rim to the apex. For $\mathrm{Re} > \mathrm{Re}_*$, the normal transfer dominates, increases circulation of the particle beyond the conservation value, and provides the positive feedback needed for the instability. In other words, due to viscous diffusion from the axis, a part of the angular momentum (that fluid transports from the near-capillary region) does not return with the fluid

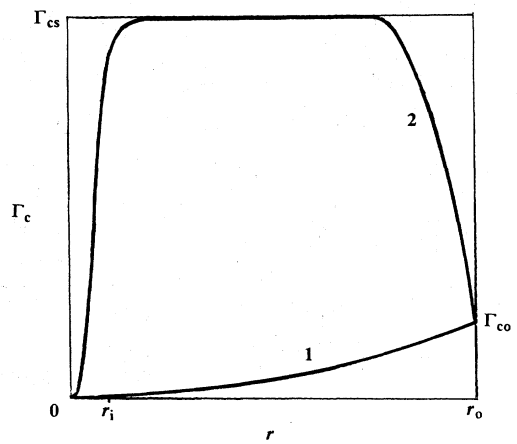

FIG. 9. Distribution of circulation at the surface Γ_c at distance r from the cone apex for $\mathrm{Re} \ll \mathrm{Re}_*$ (curve 1) and for $\mathrm{Re} > \mathrm{Re}_*$ (curve 2). Γ_{co} represents circulation near the capillary rim, Γ_{cs} the self-similar value of Γ_c.

flow and, therefore, the angular momentum accumulates inside the cone. Curve 2 in the vicinity of $r = r_o$ in Fig. 9 shows this growth of circulation due to the instability as r decreases.

The nonlinear saturation of circulation occurs due to the fact that the growth of the meridional transfer is less than the growth of the radial one when Γ_c is large and increases. The reason is that the meridional motion becomes relatively weaker, spending its energy to increase rotation (see Fig. 5). As a result, when circulation becomes great enough, the diffusion fluxes in the meridional and radial directions again reach balance and circulation is established, i.e., becomes independent of r, which corresponds to the secondary similarity solution (see the middle part of curve 2 in Fig. 9 where $\Gamma_c \cong \Gamma_{cs}$, Γ_{cs} is the similarity value). In the vicinity $r < r_i$ of the cone apex, the similarity solution cannot be applied because there is a stagnation point. Since the meridional motion becomes slow in this vicinity, solid-body rotation is expected (see curve 2 in the vicinity $r = 0$ in Fig. 9).

It is worth emphasizing that the saturation value of circulation (Γ_{cs}) does not depend on the disturbance amplitude Γ_{co} at $r = r_o$. In this sense, the secondary similarity solution is self-swirling but not forced. The forcing at $r = r_o$ serves just as a trigger for the instability process.

B. Analogy with the axisymmetric hydromagnetic dynamo

For the same conical similarity class, the axisymmetric hydromagnetic dynamo (AHD) i.e., appearance of the magnetic induction through a bifurcation in the primarily nonmagnetic flow of viscous incompressible electrically conducting fluid, has been found [13–15]. Although AHD does not contradict Cowling's and Braginsky's "antidynamo" theorems, since the theorem conditions are not fulfilled, nevertheless AHD is not related to local generation of the magnetic field but to a special exchange with a weak outer source of induction. Based on the above results, we can assume that the instability mechanism for AHD is similar to that for the swirl dynamo. For both these cases, one needs the circulatory meridional motion with an inflow near a conical surface and an outflow near the axis. Also, diffusion in the normal-to-axis direction plays a crucial role, but the diffusion is magnetic in the AHD case. The induction accumulation is not due to a simple mechanical transport of magnetic lines to the origin by the converging flow, but induction grows beyond its conservation value due to the instability mechanism that is similar to the swirl dynamo case.

C. Comparison with the swirl bifurcation in Karman's similarity class

Appearance of swirl due to bifurcation was also found for the steady viscous flows between porous and impermeable disks [16]. Uniform suction through the porous disk induces radial inflow to the symmetry axis and there is a similarity solution of Karman's class (the normal velocity depends on the normal coordinate only, but the other components are proportional to the distance from the axis s in Karman's class). At some Re, a

secondary swirling regime appears in addition to the primary nonswirling solution. The secondary regime is also self-similar, with the solid-body-type dependence of the azimuthal velocity on s. Experiments with a forced rotation at the disk rim show that circulation decays faster than s^2 as s decreases for $\mathrm{Re} < \mathrm{Re}_*$, but there is a near-axis region where circulation is proportional to s^2 for $\mathrm{Re} > \mathrm{Re}_*$ [16].

Although the value of the angular velocity in the similarity region also does not depend on its value at the disk rim, the physical nature of bifurcation in Karman's class is quite different from that in our problem. The problem is that there is no accumulation of circulation between the disks. If one ignores the viscous transfer, then circulation transported by the inflow would be constant along streamlines and equal to its ambient value. Viscous losses of the angular momentum at the walls due to the no-slip condition, together with diffusion in the radial direction, can only decrease circulation downstream. This decrease is very fast for $\mathrm{Re} \ll \mathrm{Re}_*$ but the solid-body rotation is established in the secondary regime for $\mathrm{Re} > \mathrm{Re}_*$ as convection compensates for viscous diffusion in the normal direction. When circulation at the rim is larger than the similarity value, then it decreases with s faster than $\sim s^2$ until it reaches the similarity value. When circulation at the rim is less than the similarity value, then it decreases more slowly than $\sim s^2$ until it reaches the similarity value. Therefore, circulation always decreases downstream in the flow between the disks while circulation increases due to the instability in our case.

X. CONCLUSION

Our stability analysis reveals the nature of the appearance of the self-swirling regime in Taylor cones. The source of swirl is positioned in the near-capillary region and for small Re induces the solid-body-type rotation in the meniscus. However, when Re exceeds its critical value, the angular momentum accumulates inside the cone up to its value corresponding to the secondary similarity solution. This saturation value does not depend on and can be drastically larger than the near-capillary circulation. The accumulation is due to the circulatory character of the meridional motion converging toward the apex near the surface and to viscous diffusion of the angular momentum from the cone axis.

[1] J. Zeleny, Phys. Rev. **10**, 1 (1917).
[2] G. I. Taylor, Proc. R. Soc. London **280A**, 383 (1964).
[3] J. Fernandez de la Mora, J. Fluid Mech. **243**, 561 (1992).
[4] L. Hayati, A. I. Bailey, and Th. F. Tadros, Nature **319**, 41 (1986).
[5] V. Shtern and A. Barrero, J. Aerosol Sci. **25**(6), 1049 (1994).
[6] V. Shtern, M. Goldshtik, and F. Hussain, Phys. Rev. E **49**, 2881 (1994).
[7] M. A. Goldshtik and V. N. Shtern, J. Fluid Mech. **218**, 483 (1990).
[8] V. I. Yudovich, Dok. Akad. Nauk SSSR **161**, 1037 (1965) [Sov. Phys. Dokl. **10**, 293 (1965)].
[9] D. D. Joseph, *Stability of Fluid Motion* (Springer, New York, 1976), Part 1.
[10] W. H. H. Banks, P. G. Drazin, and M. B. Zaturska, J. Fluid Mech. **186**, 559 (1988).
[11] M. Goldshtik, F. Hussain, and V. Shtern, J. Fluid Mech. **232**, 521 (1991).
[12] M. Cloupeau and B. Prunet-Foch, J. Electrostatics **22**, 135 (1989).
[13] M. A. Goldshtik and V. N. Shtern, Zh. Eksp. Teor. Fiz. **96**, 1728 (1989) [Sov. Phys. JETP **69**, 975 (1989)].
[14] M. A. Goldshtik and V. N. Shtern, Prog. Astronaut. Aeronaut. **149**, 87 (1993).
[15] A. A. Petrunin and V. N. Shtern, Prog. Astronaut. Aeronaut. **149**, 116 (1993).
[16] M. A. Goldshtik and N. I. Javorsky, J. Fluid. Mech. **207**, 1 (1989).

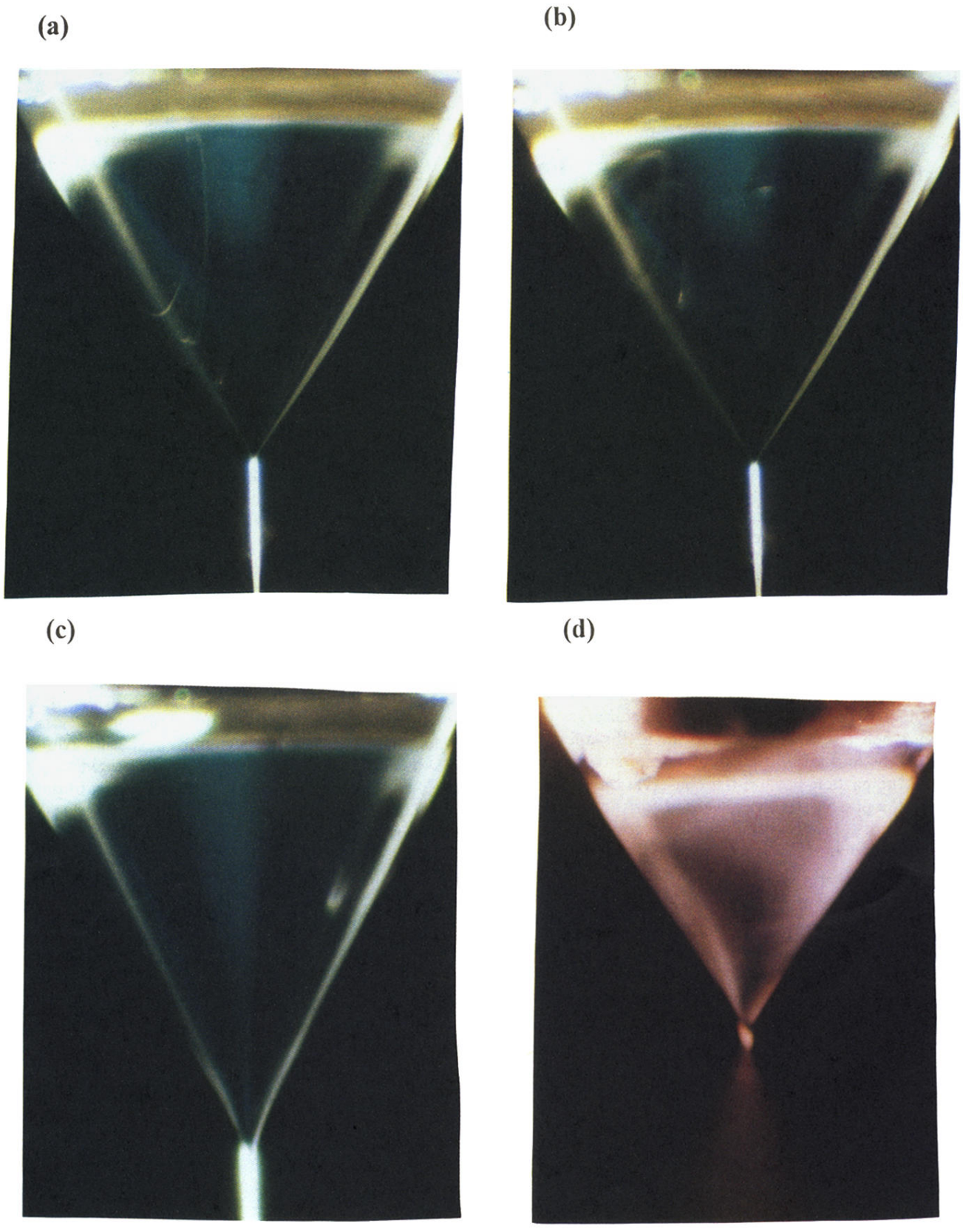

FIG. 7. Photographs of the nonswirling (a) and swirling (b)–(d) regimes in a Taylor cone.